Experimental Section

Synthesis of MOFs

$Zn(NO_3)_2 \cdot 6H_2O$ (1.5 mmol) and $Co(NO_3)_2 \cdot 6H_2O$ (1.5 mmol) were dissolved in 12 mL of methanol to form a clear solution A. 2-methylimidazole (2-MeIM, 12 mmol) was dissolved in 20 mL of methanol to form another clear solution B. Solution A was then added to the solution B under continuous stirring for 5 min and kept for 12 h. Then, the precipitate, named as ZIF-Zn/Co(1:1), was collected, washed with methanol several times, and dried under a vacuum. For the syntheses of ZIF-Zn/Co(1:0) and ZIF-Zn/Co(0:1), the amounts of $Zn(NO_3)_2 \cdot 6H_2O$ and $Co(NO_3)_2 \cdot 6H_2O$ were adjusted to 3.0 mmol : 0 mmol and 0 mmol : 3 mmol, respectively.

Characterization

Crystal structures of the samples were characterized by powder X-ray diffraction (XRD, Ultima Rint 2000 X-ray diffractometer, RIGAKU, Japan) using Cu Kα radiation (40 kV, 40 mA, $2^\circ\,min^{-1}$ scan rate). The morphologies of the resulting samples were observed by field-emission scanning electron microscopy (FESEM, HITACHI SU8000). The N_2 adsorption–desorption isotherms were obtained using BELSORP-max (BEL, Japan), which was used to measure the specific surface areas of the samples using the Brunauer–Emmett–Teller (BET) method.

Electrochemical analyses

The electrochemical measurements were conducted using an electrochemical workstation (CHI-760E) with a three-electrode system consisting of 1 M NaCl aqueous electrolyte, a platinum wire counter electrode, and an Ag/AgCl reference electrode. Cyclic voltammetry (CV) and galvanostatic charge-discharge (GCD) measurements were conducted in the potential range of –0.5 to 0.5 V. The Nyquist plots were obtained from electrochemical impedance spectroscopy measurements in the frequency range of 10 mHz to 100 kHz.

The specific capacitances were calculated from the discharge curves using the following equation:

$$C = i \times t/\Delta V \quad (1)$$

where i is the discharge current density (A g^{-1}), t is the discharge time (s), and ΔV is the voltage window (V).

Desalination analysis

Each individual capacitive deionization (CDI) electrode was fabricated by depositing a mixture of the sample, carbon black, and poly(vinylidene fluoride) binder with a weight ratio of 8:1:1 on a graphite paper (2 × 2 cm^2), and dried under vacuum at 60 °C for 12 h.

The CDI tests were conducted using a batch mode with a continuous recycling system, which consists of a pair of anion- and cation-exchange membranes, peristaltic pump, power source, and tank. The real-time saline concentration variation was monitored and measured using an ion conductivity meter. The volume of the saline solution was fixed to 30 mL, the flow rate was 30 mL min^{-1}, and the operating voltage was 1.2 V.

The SAC (mg g^{-1}) and SAR (mg g^{-1} min^{-1}) at t min were calculated as follows:

$$SAC = (C_0 - C_t) \times V/m \quad (2)$$

$$SAR = SAC/t \quad (3)$$

where C_0 and C_t are the concentrations of NaCl at the initial stage and t min, respectively (mg L^{-1}), V is the volume of the NaCl solution (L), and m is the total mass of the electrode materials (g).

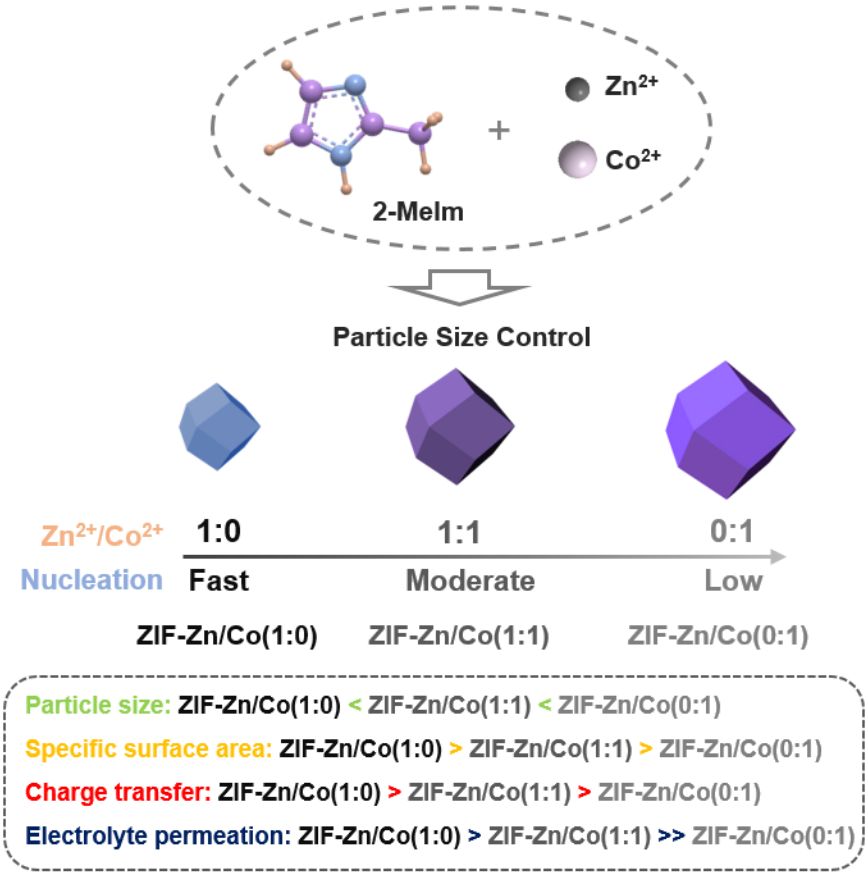

Fig. S1 Particle size control of ZIFs for optimizing their physicochemical properties.

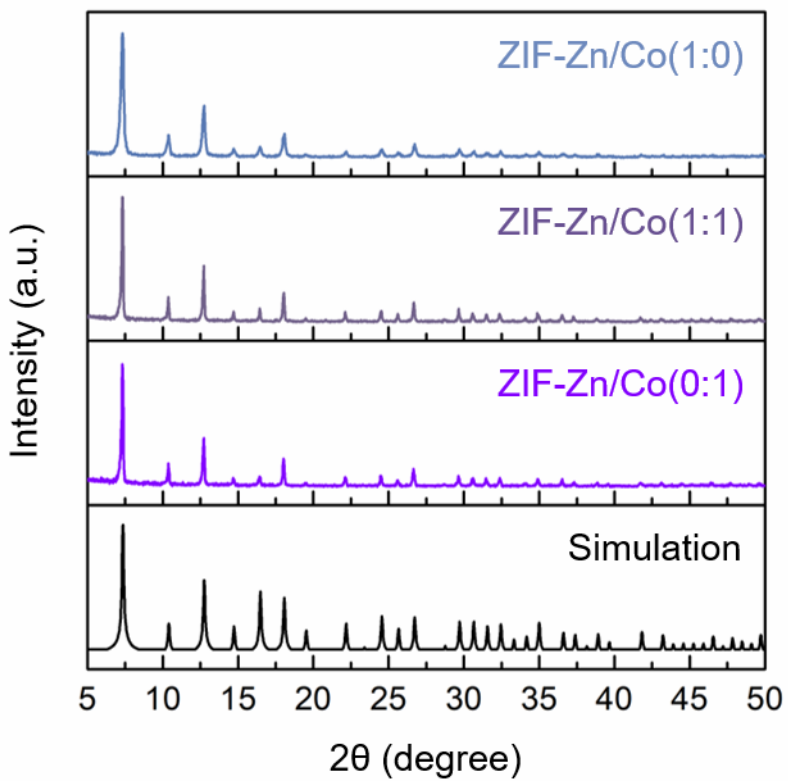

Fig. S2 XRD patterns of the prepared MOF particles.

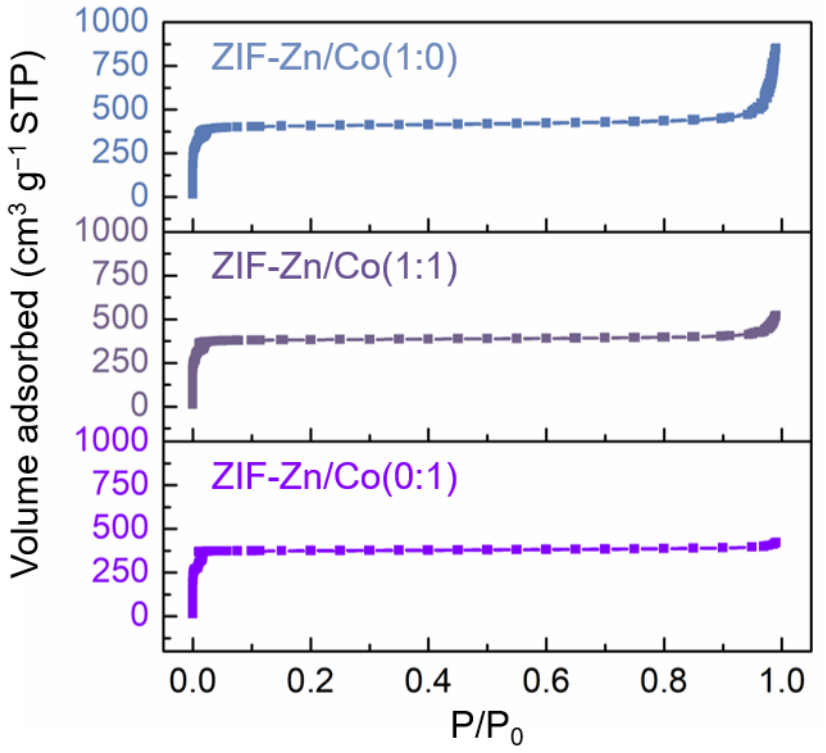

Fig. S3 N_2 adsorption–desorption isotherms of the MOF particles.

Supplementary Note for Fig. S3: Regardless of the particle sizes, all MOF particles exhibit Type-I isotherms, suggesting they have microporous structures. Furthermore, the particle size decreases in the following order of ZIFs: ZIF-Zn/Co(1:0) > ZIF-Zn/Co(1:1) > ZIF-Zn/Co(0:1); consequently, the specific surface areas decrease from 1619.6 $m^2 g^{-1}$ to 1560.7 $m^2 g^{-1}$, and 1459.7 $m^2 g^{-1}$, respectively.

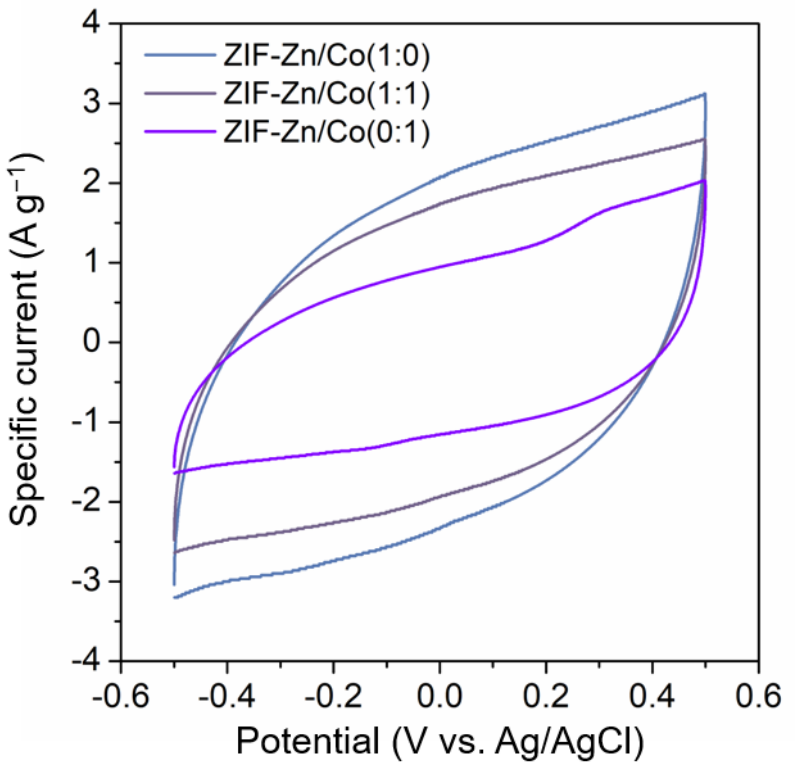

Fig. S4 CV curves of the MOF particles in 1 M NaCl at 10 mV s^{-1}.

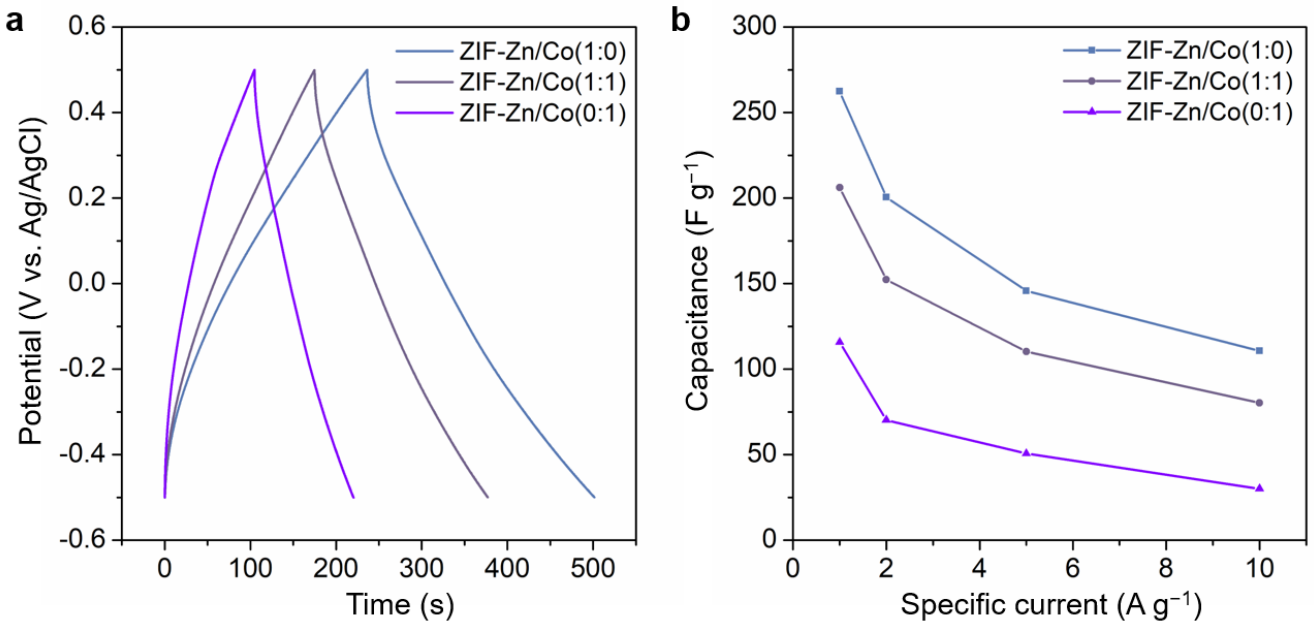

Fig. S5 Curves of (a) GCD and (b) capacitances versus specific currents of the MOF particles.

Table S1 Fitting coefficients of the Langmuir isotherms of the ZIFs for the CDI profiles at various concentrations.

Isotherm	Model equation	Sample	Parameter	Value
Langmuir	$q = \frac{q_m K_L C}{1 + K_L C}$	ZIF-Zn/Co(1:0)	q_m	28.54
			K_L	0.08613
			r^2	0.996
		ZIF-Zn/Co(1:1)	q_m	22.43
			K_L	0.00564
			r^2	0.997
		ZIF-Zn/Co(0:1)	q_m	11.88
			K_L	0.05002
			r^2	0.985

Supplementary Note for Fig. 2d and Table S1: The electrosorption isotherm correlates with the NaCl concentration in the bulk solution and SAC of the electrode.[1] Analysis of the isotherm data is important for developing an equation that accurately represents the results. In this study, the Langmuir isotherm model was used to simply simulate the experimental data for the CDI process, as shown in **Table S1**. We admit that the Langmuir isotherm might not be a good tool for accurate analysis of changes in the desalination behavior with respect to saline concentration. However, to simplify the simulations of the experimental data and obtain a preliminary trend for SAC versus saline concentration, the Langmuir isotherm was used for performance evaluation as described by the following equation:

$$q = \frac{q_m K_L C}{1+K_L C} \quad (4)$$

where q is the SAC (mg g^{-1}), q_m is the maximum SAC (mg g^{-1}), C is the equilibrium concentration (ppm), and K_L is the Langmuir constant related to the free energy of the CDI process. The simulated linear fit and coefficients are presented in **Fig. 2d** and **Table S1**, respectively.

Table S2 Comparisons of SAC/SSAs (mg m^{-2}) derived from **Fig. 2c-d**.

Voltage (V)	**ZIF-Zn/Co(1:0)**	**ZIF-Zn/Co(1:1)**	**ZIF-Zn/Co(0:1)**	**Concentration (mM)**	**ZIF-Zn/Co(1:0)**	**ZIF-Zn/Co(1:1)**	**ZIF-Zn/Co(0:1)**
0.6	0.0028	0.0013	0.0009	**5**	0.0053	0.0037	0.0014
0.8	0.0043	0.0032	0.0014	**10**	0.0083	0.0062	0.0028
1	0.0060	0.0049	0.0020	**20**	0.0109	0.0084	0.0042
1.2	0.0083	0.0062	0.0028	**40**	0.0138	0.0107	0.0054

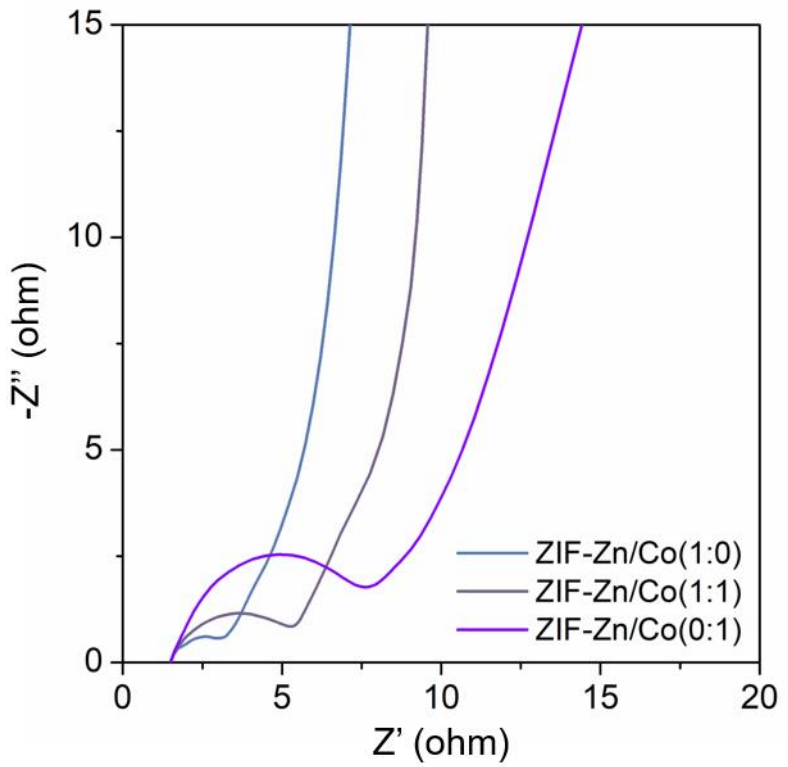

Fig. S6 Nyquist plots of MOF particles.

Table S3 R_{ct} values of MOF particles.

Sample	R_{ct} (ohm)
ZIF-Zn/Co(1:0)	2.2
ZIF-Zn/Co(1:1)	4.3
ZIF-Zn/Co(0:1)	6.7

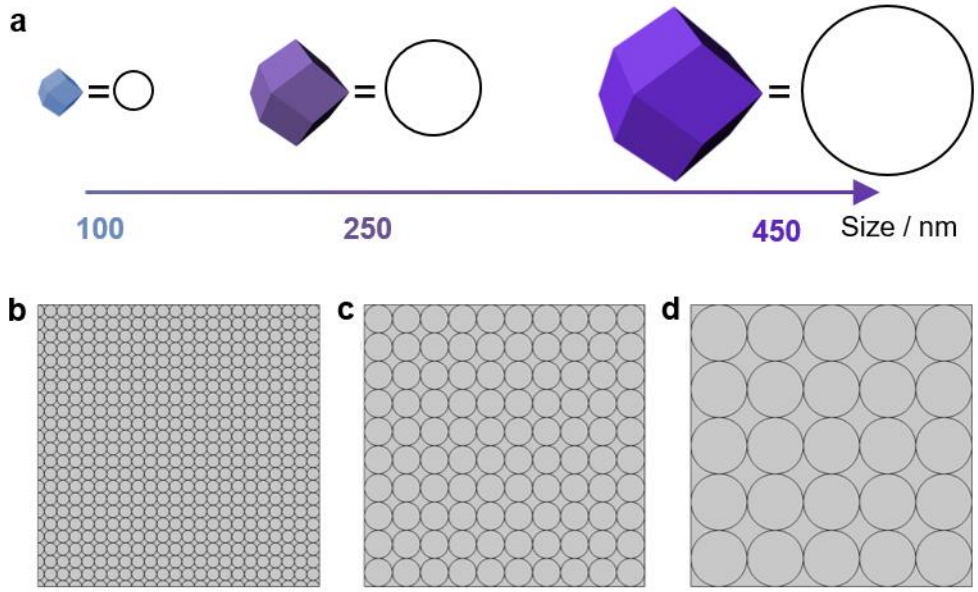

Fig. S7 Schemes for (a) model evolution of the MOF particles and (b-c) corresponding stacked particle models with sizes of (b) 100 nm, (c) 250 nm, and (d) 450 nm.

Supplementary Note for Fig. S7: We have rationally designed two-dimensional axisymmetric models for finite element simulations (**Fig. S7**). Then, we applied Fick's second law to simulate the calculation domain (the gray area in the geometric model) and calculated the diffusion flux density (amount of ions in dimension per unit area per unit time transporting through the electrodes) to evaluate the internal ion transport rate of the electrode. Fick's second law is as follows:

$$\frac{\partial C_0}{\partial t} = D_0 \nabla^2 C_0 \tag{5}$$

where C_0 is the concentration of dimensions, t is the time, and D_0 is the diffusion coefficient in dimensions. We assumed that the calculation domain was filled with a certain concentration gradient of the NaCl solution. The ion transport distance in the electrode was set to be the width of the model (2.25 μm). Based on the desalination performance of the NaCl solution, the salt concentration of the model at the inlet was set to be 10 mM. The temperature and NaCl diffusion rate in the simulations were 298 K and 2.03×10^{-9} m^2 s^{-1}, respectively, and the boundary conditions are summarized in **Table S4**.

Table S4 Boundary conditions for finite element simulations.

Boundary	Description
Inlet	c_i=10 mM
Insulating	$-n.J_i = 0$
Outlet	c_i=0 mM
Insulating	$-n.J_i = 0$

$$\nabla^2 V = \begin{cases} 0 & d < d_H \\ (C_{Na} - C_{Cl})F & d > d_H \end{cases} \quad (6)$$

$$\nabla \cdot (D\nabla c_i + \frac{Dz_i e}{k_B T} c_i \nabla V) = 0 \quad (7)$$

where d represents the distance from the electrode surface to the electrolyte, c_i is the concentration of a sodium ion or a chloride ion, z_i is the valence state of ions, e is the basic charge, k_B is the Boltzmann constant, temperature T is 298 K, and d_H is the thickness of the dense layer. The thickness is obtained from the radius of a hydrated sodium ion (0.36 nm); that is, $d < d_H$ is in the dense layer, and $d > d_H$ is in the diffusion layer. Furthermore, D represents the self-diffusion coefficient of sodium ions, chloride ions, and protons in aqueous solutions. The sample model was taken from a single individual in the previous simulation.

In addition, the Millington and Quirk model was used to correct the diffusivity in porous media:

$$\tau_{F,i} = \varepsilon_p^{-1/3} \quad (8)$$

where $\tau_{F,i}$ is tortuosity, and ε_p is porosity.

Table S5 The minimum saline concentrations (mM) at each stage (0 – 0.02 s).

Particle size	0 s	0.01 s	0.02 s
100 nm	0	7.62	9.58
250 nm	0	7.29	9.45
450 nm	0	5.18	8.13

Table S6 Performance comparisons between the optimal MOF particles and other materials under optimization conditions.

Sample	Counter electrode	Concentration (mg L^{-1})	Voltage (V)	SAC (mg g^{-1})
ZIF-Zn/Co(1:0)	Same	584 N.A.	1.2	13.45 28.54
MOF/PPy[2]	Same	584 ~1530	1.2	11.34 15.3
MOF/CNT[3]	Same	300	1.2	16.90
Patterning MOFs[4]	Same	300	1.2	21.3
PDA@AC[5]	Same	500	1.2	10.43
PTMA[6]	AC	250	1.2	13.9
MT–AC[7]	HT–AC	500	1.2	15.8
CME-2/5[8]	CNT	1000	1.2	15
3-D GSSNA[9]	Same	500	1.2	22.09
3D graphene hydrogel[10]	Same	~5000	1.2	26.8
PC-900[11]	Same	500	1.2	10.90
Nitrogen-doped graphene sponge[12]	Same	500	1.2	21.04
Graphene[13]	Same	86	1.2	10.7

ECNG[13]	Same	86	1.2	18.6
G/N-CFs[14]	Same	585	1.2	27.55
GTAC[15]	Same	50	1.2	2.30
		500		10.94
Graphene/CNTs sponge[16]	Same	500	1.2	18.70
NAPC[17]	Same	1000	1.2	28.6
ANCM[18]	Same	500	1.2	13.3
N-SDG[19]	Same	500	1.2	19.6
SGO@ACF[20]	Same	500	1.2	11.66
		700		14.74
NPPC-800[21]	Same	584.4	1.2	35.7
MOF-5 carbon[22]	Same	500	1.2	9.39
ZIF-8-C[23]	Same	500	1.2	13.86
ZnFumarate carbon[24]	Same	58.44	1.2	8.1
		292.2		13.1
RT-MOF-5 carbon[24]	Same	58.44	1.2	6.3
ZIF-8 carbon[24]	Same	58.44	1.2	3.7
Hollow ZIF carbon[25]	Same	500	1.2	15.31
AC-CDI[26]	Same	2000	1.2	20.8
ZIF-8@PZS-C[27]	Same	500	1.2	22.19

MWCNT/PVA[28]	Same	58.44	1.2	13.07
nit-CNTs[29]	Same	2337.6	1.2	17.18
rGO–PS[30]	Same	400	1.2	15.93
YS-PCSs[31]	Same	1000	1.2	19.77
3DGA-OP[32]	Same	500	1.2	14.4
P-CNFA[33]	Same	1000	1.2	16.2
MMC-A[34]	Same	500	1.2	17.38
MMC[35]	Same	1000	1.4	20.78
CS + 3GA[36]	PVDF	500	1.2	16.0
			1.4	18.4
NCPCs[37]	Same	100	1.6	11.98
		250		13.57
		500		17.2
N-PHCS[38]	Same	500	1.4	12.95
		500	1.6	17.1
PAC/PTS[39]	Same	600	1.2	14.3
		600	1.4	14.9
PPy-AMC[40]	Same	1168.8	1.2	27.4
N-HMCSs[41]	Same	100	1.6	11.5
		250		13.1

		500		16.6
NPCSs[42]	Same	1000	1.2	14.91
N-doped graphene[43]	Same	50	1.8	4.81
		500	1.2	12.8
N-CNFA[44]	Same	1000	1.2	17.29
GC-2[45]	Same	584.4	1.2	16.5
AN-CFs[46]	Same	1000	1.2	16.56
Unactivated N-CFs[46]				12.02
Heteroatom-doped carbon[47]	Same	292.2	1.2	15.0
CCS[48]	Same	500	1.2	16.1
HNPC-900[49]	Same	500	1.2	21.17
NvGIII[50]	Same	500	2.0	6.52 (9.2 mg cm^{-3}; porosity: 1.41 g cm^{-3})
PCNF[51]	Same	500	1.2	23.6
MF-C[52]	Same	500	1.2	8.0
OMa[53]	Same	2000	N.A.	N.A.
3D macroporous graphene[54]	Same	50	2.0	5.39
AC-1-2.0[55]	Same	29.22	1.0	11.86
		584.4		20.91
Mesoporous graphene[56]	Same	75	1.2	6.38

3DGHPC[57]	Same	25	1.2	6.18
GNRs/CNTs[58]	Same	500	1.2	16.46
		N.A.		23.43
F–N-GPM[59]	Same	500	1.2	14.2

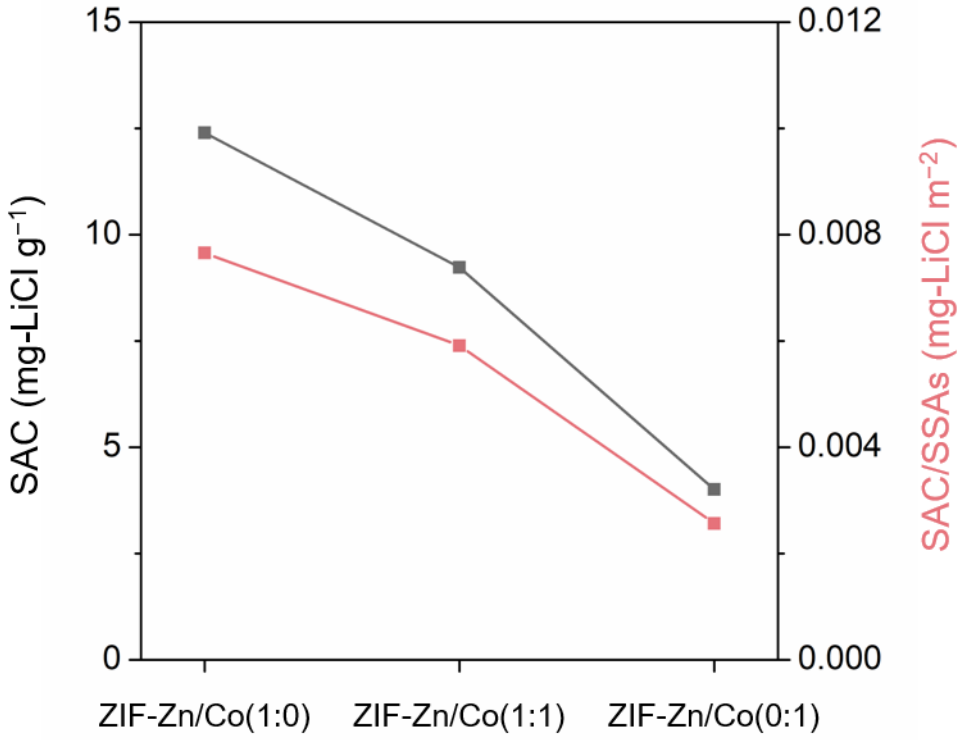

Fig. S8 SACs and SACs/SSAs for the MOF particles in a 10 mM LiCl solution at 1.2 V.

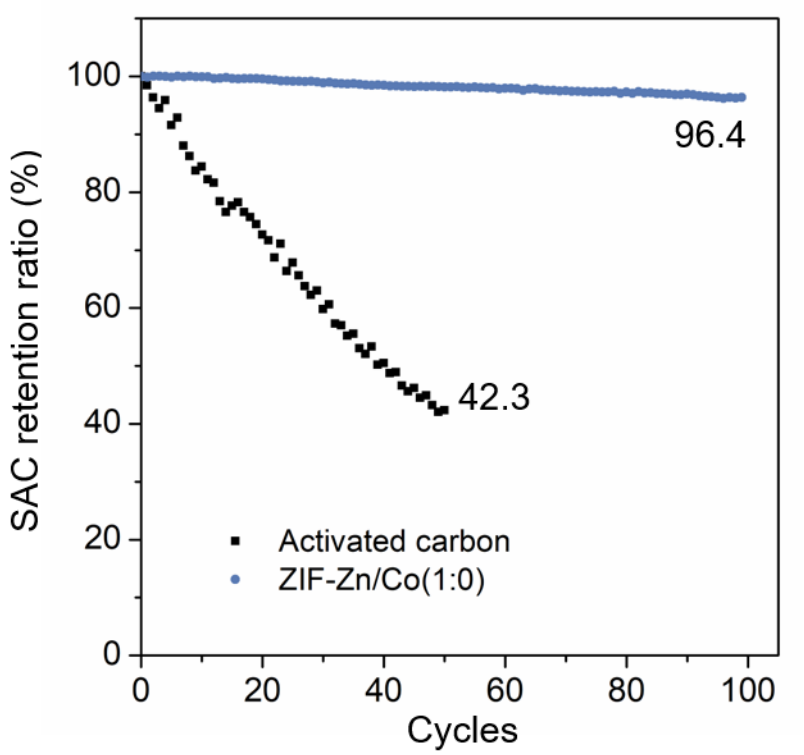

Fig. S9 Cycling SAC retention of ZIF-Zn/Co(1:0) and activated carbon in oxygenated saline water (10 mM) at 1.2 V.

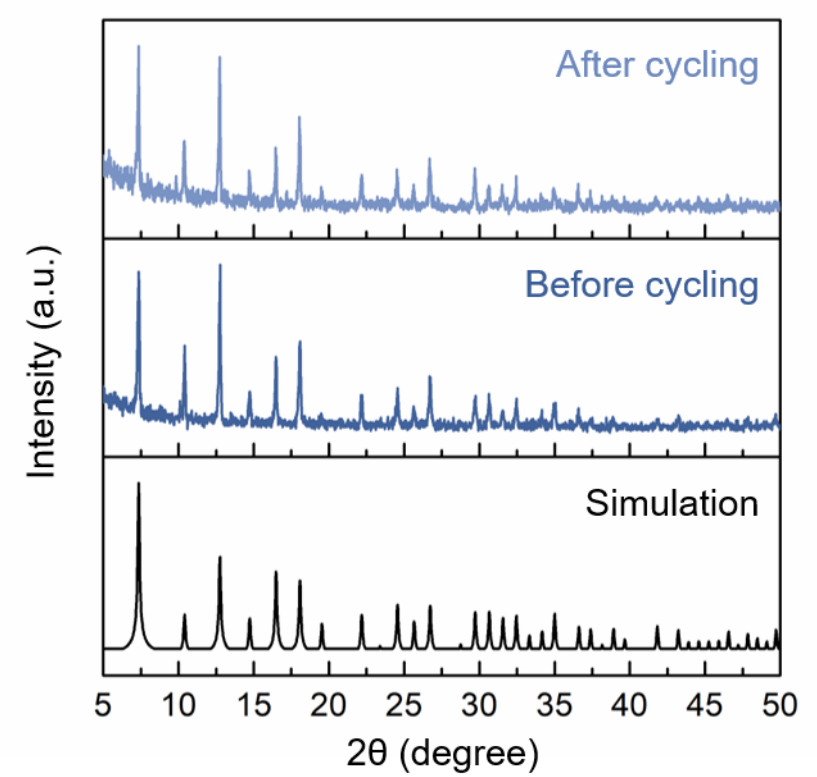

Fig. S10 XRD patterns of the ZIF-Zn/Co(1:0) electrode before and after cycling.

References

1. S. Porada, R. Zhao, A. Van Der Wal, V. Presser and P. Biesheuvel, *Prog. Mater. Sci.*, 2013, **58**, 1388-1442.
2. Z. Wang, X. Xu, J. Kim, V. Malgras, R. Mo, C. Li, Y. Lin, H. Tan, J. Tang, L. Pan, Y. Bando, T. Yang and Y. Yamauchi, *Mater. Horiz.*, 2019, **6**, 1433-1437.
3. X. Xu, C. Li, C. Wang, L. Ji, Y. V. Kaneti, H. Huang, T. Yang, K. C. W. Wu and Y. Yamauchi, *ACS Sustainable Chem. Eng.*, 2019, **7**, 13949-13954.
4. Y. Zhang, L. Ji, Y. Zheng, H. Liu and X. Xu, *Sep. Purif. Technol.*, 2020, **234**, 116124.
5. N. A. T. Tran, N. M. Phuoc, T. M. Khoi, H. B. Jung, N. Cho, Y.-W. Lee, E. Jung, B.-G. Kang, K. Park, J. Hong, C.-Y. Yoo, H. S. Kang and Y. Cho, *Appl. Surf. Sci.*, 2022, **579**, 152154.
6. Y. Li, Z. Ding, J. Li, K. Wang, T. Lu and L. Pan, *Desalination*, 2020, **481**, 114379.
7. Q. Wu, D. Liang, S. Lu, J. Zhang, H. Wang, Y. Xiang and D. Aurbach, *ACS Appl. Mater. Interfaces*, 2021, **13**, 46537-46548.
8. S. Xiong, L. Ren, C. Zhang, J. Zhou and Y. Wang, *Desalination*, 2021, **520**, 115368.
9. Z. U. Khan, T. Yan, L. Shi and D. Zhang, *Environ. Sci.: Nano*, 2018, **5**, 980-991.
10. W. Kong, X. Duan, Y. Ge, H. Liu, J. Hu and X. Duan, *Nano Res.*, 2016, **9**, 2458-2466.
11. X. Duan, W. Liu and L. Chang, *J. Taiwan Inst. Chem. E.*, 2016, **62**, 132-139.
12. X. Xu, Z. Sun, D. H. Chua and L. Pan, *Sci. Rep.*, 2015, **5**, 11225.
13. A. M. Abdelkader and D. J. Fray, *Nanoscale*, 2017, **9**, 14548-14557.
14. Y. Belaustegui, S. Zorita, F. Fernández-Carretero, A. García-Luis, F. Pantò, S. Stelitano, P. Frontera, P. Antonucci and S. Santangelo, *Desalination*, 2018, **428**, 40-49.
15. G. Zhu, W. Wang, X. Li, J. Zhu, H. Wang and L. Zhang, *RSC Adv.*, 2016, **6**, 5817-5823.
16. X. Xu, Y. Liu, T. Lu, Z. Sun, D. H. C. Chua and L. Pan, *J. Mater. Chem. A*, 2015, **3**, 13418-13425.
17. K. Liu, B. Chen, A. Feng, J. Wu, X. Hu, J. Zhou and Y. Yu, *Desalination*, 2022, **526**, 115461.
18. Z. Pei, J. Zhou, X. Xu, J. Liu, H. Wang, Y. Li, Q. Chen and Z. Sui, *J. Porous Mater.*, 2022, **29**, 415–422. .
19. O. Noonan, Y. Kong, Y. Liu, M. Kalantari, A. Kumar Nanjundan, X. Huang and C. Yu, *Adv. Energy Sustainability Res.*, **3**, 2100190.
20. L. Men, C. Chen, A. Liu, J. Zhou, S. Yu and Z. Wei, *Ionics*, 2022, **28**, 1903–1913.
21. W. Zhang, C. Jin, Z. Shi, L. Zhu, L. Chen, Y. Liu and H. Zhang, *Chemosphere*, 2022, **291**, 133113.
22. L. Chang, J. Li, X. Duan and W. Liu, *Electrochim. Acta*, 2015, **176**, 956-964.
23. Y. Liu, X. Xu, M. Wang, T. Lu, Z. Sun and L. Pan, *Chem. Commun.*, 2015, **51**, 12020-12023.
24. M. Wang, X. Xu, Y. Liu, Y. Li, T. Lu and L. Pan, *Carbon*, 2016, **108**, 433-439.
25. J. Shen, Y. Li, C. Wang, R. Luo, J. Li, X. Sun, J. Shen, W. Han and L. Wang, *Electrochim. Acta*, 2018, **273**, 34-42.
26. N. Li, J. An, X. Wang, H. Wang, L. Lu and Z. J. Ren, *Desalination*, 2017, **419**, 20-28.
27. J. Zhang, J. Fang, J. Han, T. Yan, L. Shi and D. Zhang, *J. Mater. Chem. A*, 2018, **6**, 15245-15252.
28. C.-H. Hou, N.-L. Liu, H.-L. Hsu and W. Den, *Sep. Purif. Technol.*, 2014, **130**, 7-14.
29. P. Shi, C. Wang, J. Sun, P. Lin, X. Xu and T. Yang, *Sep. Purif. Technol.*, 2020, **235**, 1903–1913.
30. M. R. Islam, S. S. Gupta, S. K. Jana, P. Srikrishnarka, B. Mondal, S. Chennu, T. Ahuja, A. Chakraborty and T. Pradeep, *Adv. Mater. Interfaces*, 2021, **8**, 2001998.
31. X. Wei, X. Li, C. Lv, X. Mo and K. Li, *Electrochim. Acta*, 2020, **354**, 136590.
32. Y. Zhu, G. Zhang, C. Xu and L. Wang, *ACS Appl. Mater. Interfaces*, 2020, **12**, 29706-29716.
33. Y. Li, Y. Liu, M. Wang, X. Xu, T. Lu, C. Q. Sun and L. Pan, *Carbon*, 2018, **130**, 377-383.
34. S. Zhao, T. Yan, Z. Wang, J. Zhang, L. Shi and D. Zhang, *RSC Adv.*, 2017, **7**, 4297-4305.
35. D. Xu, Y. Tong, T. Yan, L. Shi and D. Zhang, *ACS Sustainable Chem. Eng.*, 2017, **5**, 5810-5819.
36. J. Weng, S. Wang, G. Wang, P. Zhang, B. Lu, H. Wang, J. Jiang and C. Li, *Desalination*, 2021, **505**, 114979.

37. Y. Li, Y. Liu, J. Shen, J. Qi, J. Li, X. Sun, J. Shen, W. Han and L. Wang, *Desalination*, 2018, **430**, 45-55.
38. S. Zhao, T. Yan, H. Wang, G. Chen, L. Huang, J. Zhang, L. Shi and D. Zhang, *Appl. Surface Sci.*, 2016, **369**, 460-469.
39. R. L. Zornitta, F. J. García-Mateos, J. J. Lado, J. Rodríguez-Mirasol, T. Cordero, P. Hammer and L. A. M. Ruotolo, *Carbon*, 2017, **123**, 318-333.
40. F. Ji‡, L. Wang‡, J. Yang, X. Wu, M. Li, S. Jiang, S. Lin and Z. Chen, *J. Mater. Chem. A*, 2019, **7**, 1768-1778.
41. Y. Li, J. Qi, J. Li, J. Shen, Y. Liu, X. Sun, J. Shen, W. Han and L. Wang, *ACS Sustainable Chem. Eng.*, 2017, **5**, 6635-6644.
42. Y. Liu, T. Chen, T. Lu, Z. Sun, D. H. C. Chua and L. Pan, *Electrochim. Acta*, 2015, **158**, 403-409.
43. X. Xu, L. Pan, Y. Liu, T. Lu and Z. Sun, *J. Colloid Interface Sci.*, 2015, **445**, 143-150.
44. G. Zhu, H. Wang, H. Xu and L. Zhang, *Jo. Electroanal. Chem.*, 2018, **822**, 81-88.
45. Z. Xie, X. Shang, K. Xu, J. Yang, B. Hu, P. Nie, W. Jiang and J. Liu, *J. Electrochem. Soc.*, 2019, **166**, E240-E247.
46. L. Zhang, Y. Liu, T. Lu and L. Pan, *J. Electroanal. Chem.*, 2017, **804**, 179-184.
47. S. Porada, F. Schipper, M. Aslan, M. Antonietti, V. Presser and T. P. Fellinger, *ChemSusChem*, 2015, **8**, 1867-1874.
48. G.-X. Li, P.-X. Hou, S.-Y. Zhao, C. Liu and H.-M. Cheng, *Carbon*, 2016, **101**, 1-8.
49. M. Zong, S. Huo, Y. Liu, X. Zhang and K. Li, *Sep. Purif. Technol.*, 2021, **256**, 117818.
50. Y. Li, N. Chen, Z. Li, H. Shao, X. Sun, F. Liu, X. Liu, Q. Guo and L. Qu, *Adv. Mater.*, 2021, **33**, 2105853.
51. L. Szabó, X. Xu, K. Uto, J. Henzie, Y. Yamauchi, I. Ichinose and M. Ebara, *ACS Appl. Mater. Interfaces*, 2022, **14**, 4004-4021.
52. T. Hussain, P. Nie, B. Hu, X. Shang, J. Yang and J. Liu, *J. Mater. Sci.*, 2021, **56**, 10282-10292.
53. L. Liu, C. Zhao, F. Zheng, D. Deng, M. A. Anderson and Y. Wang, *Desalination*, 2021, **498**, 114794.
54. H. Wang, D. Zhang, T. Yan, X. Wen, J. Zhang, L. Shi and Q. Zhong, *J. Mater. Chem. A*, 2013, **1**, 11778-11789.
55. C.-L. Yeh, H.-C. Hsi, K.-C. Li and C.-H. Hou, *Desalination*, 2015, **367**, 60-68.
56. X. Xu, Y. Liu, M. Wang, X. Yang, C. Zhu, T. Lu, R. Zhao and L. Pan, *Electrochim. Acta*, 2016, **188**, 406-413.
57. X. Wen, D. Zhang, T. Yan, J. Zhang and L. Shi, *J. Mater. Chem. A*, 2013, **1**, 12334-12344.
58. H. Wang, W. Sun, Y. Liu, H. Ma, T. Li, K. A. Lin, K. Yin and S. Luo, *J. Electroanal. Chem.*, 2022, **904**, 115907.
59. G. Zhang, W. Li, Z. Chen, J. Long and C. Xu, *Carbon*, 2022, **187**, 86-96.